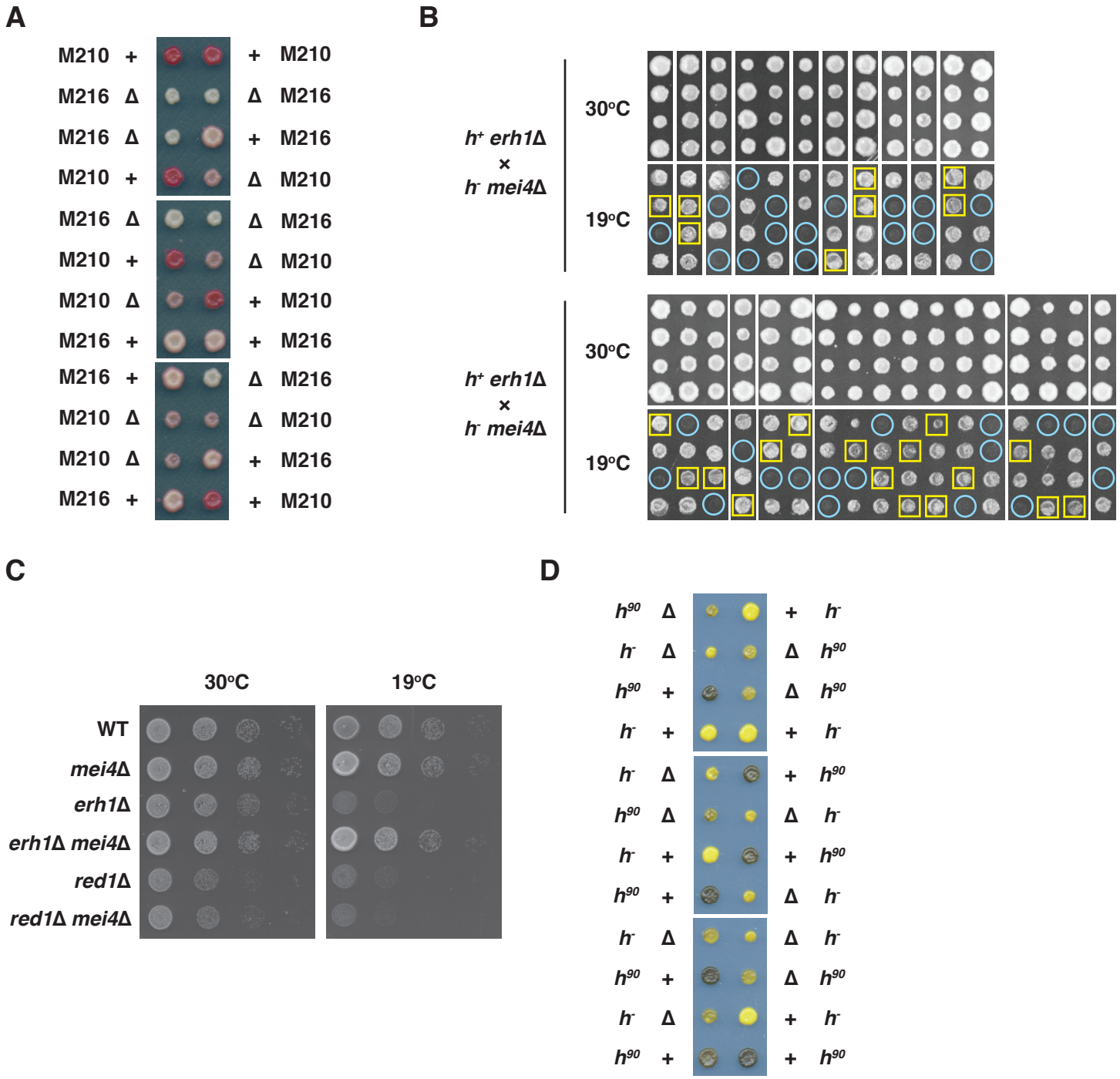

Figure S1. Phenotypes associated with *erh1*Δ, related to Figure 1

(A) *erh1*Δ affects the *ade6* phenotype. Tetrad dissection of *erh1*Δ (Δ) *ade6-M210* × *erh1*$^{+}$ (+) *ade6-M216*. Dissected spores were grown on rich plates, and then replica plated and grown on adenine-deficient plates. (B) *erh1*Δ *mei4*Δ but not *erh1*Δ grows at 19°C. Tetrad dissection of *erh1*Δ *ade6-M210* × *mei4*Δ *ade6-M216* and *erh1*Δ *ade6-M216* × *mei4*Δ *ade6-M210*. Dissected spores were grown on rich (YEA) plates at 30°C, and then replicated and grown on YEA plates at the indicated temperatures. Light blue circles, *erh1*Δ; yellow squares, *erh1*Δ *mei4*Δ. (C) *mei4*Δ suppresses the cold-sensitivity of *erh1*Δ, but not *red1*Δ. Ten-fold serial dilutions of each strain were spotted on rich (YEA) plates and then incubated at the indicated temperatures.(D) *erh1*Δ affects sporulation as indicated by iodine staining intensity. Tetrad dissection of *h*^{90} *erh1*Δ (Δ) × *h*$^{-}$ *erh1*$^{+}$ (+). Dissected spores were grown on rich plates, and then replica plated and grown on minimal plates to induce sporulation, followed by exposure to iodine vapor.

A

class	#
transient	19
continuous	18
delayed	7
early	43
middle	91
late	15
N.A.	30
total	223

B

Gene ontology	#
meiotic nuclear division	48
meiotic cell cycle	46
cytoplasmic translation	44
transmembrane transport	41
signaling	32
DNA recombination	30
transcription, DNA-templated	30
chromosome segregation	21
cytoskeletal organization	20
nucleobase-containing small molecule metabolic process	20

C

class of non-coding RNAs	#
antisense RNA	31
non-coding RNA	29
tRNA	26
intergenic RNA	20
intergenic RNA, possible alternative UTR	19
non coding RNA, poly(A)-bearing	9
small nucleolar RNA	6
18S rRNA	5
tRNA, mitochondrial	5
antisense RNA, possible alternative UTR	5
28 rRNA	3
meiRNA	1
total	159

D

class	#
transient	3
continuous	0
delayed	3
early	1
middle	0
late	2
N.A.	3
total	13

E

Gene ontology	#
cytoplasmic translation	66
transmembrane transport	12
mitochondrion organization	9
ribosome biogenesis	5
snoRNA metabolic process	4
cellular amino acid metablic process	4
transcription, DNA-templated	4
protein complex assembly	3
nucleobase-containing small molecule metabolic process	3
carbohydrate metabolic process	2
cell adhesion	2
tRNA metabolic process	2
mRNA catabolic process	2

F

class of non-coding RNAs	#
antisense RNA	80
intergenic RNA	55
tRNA	40
5S rRNA	31
non-coding RNA	28
antisense RNA, possible alternative UTR	21
small nucleolar RNA	17
intergenic RNA, possible alternative UTR	6
ncRNA, poly(A)-bearing	5
tRNA, mitochondrial	5
21S rRNA, mitochondrial	1
15S rRNA, mitochondrial	1
total	290

Figure S2. Expression profile analysis of *erh1*Δ, related to Figure 2

(A) Meiotic genes upregulated in vegetative *erh1*Δ are classified according to their expression patterns. N.A., not assigned but increased during meiosis. (B) GO (Gene ontology) analysis of upregulated genes in vegetative *erh1*Δ cells. Ten GO terms are shown in the list. Note “meiotic cell cycle” is the GO term (biological process) and the others are GO slim terms. (C) Classification of accumulated non-coding RNAs in *erh1*Δ. (D) Meiotic genes downregulated in vegetative *erh1*Δ cells are classified according to their expression patterns. N.A., not assigned but increased during meiosis. (E) GO analysis of downregulated genes in vegetative *erh1*Δ. Thirteen GO terms are shown in the list. (F) Classification of non-coding RNAs that are decreased in *erh1*Δ.

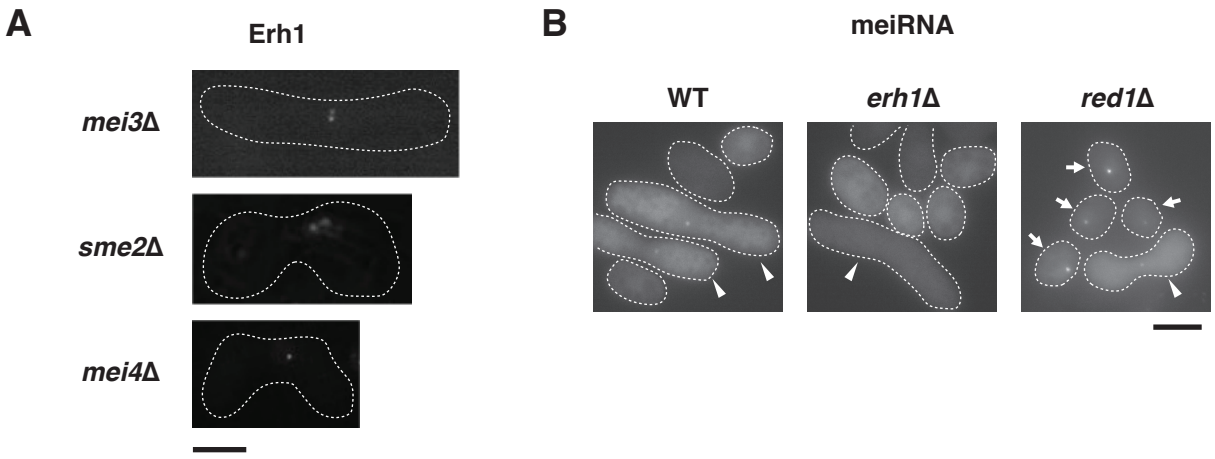

Figure S3. Erh1 localization and meiRNA dot analysis in various deletion cells, related to Figure 3
(A) Meiosis was induced in homothallic *mei3*Δ, *sme2*Δ or *mei4*Δ cells expressing Erh1-GFP, and the localization of Erh1-GFP in these strains was analyzed by fluorescence microscopy. Representative images are shown, and the white dashed lines indicate the cell shape. Bars, 5 μm. (B) The meiRNA dot is observed in meiotic wild-type and *red1*Δ cells, but is also observed in mitotic *red1*Δ cells. Meiosis was induced in homothallic wild-type (WT), *erh1*Δ and *red1*Δ cells expressing MS2 loop tagged meiRNA and MS2-GFP, and the formation of the meiRNA dot in these strains was examined by fluorescence microscopy. Representative images are shown, and the white dashed lines indicate the cell shape. Bars, 5 μm.

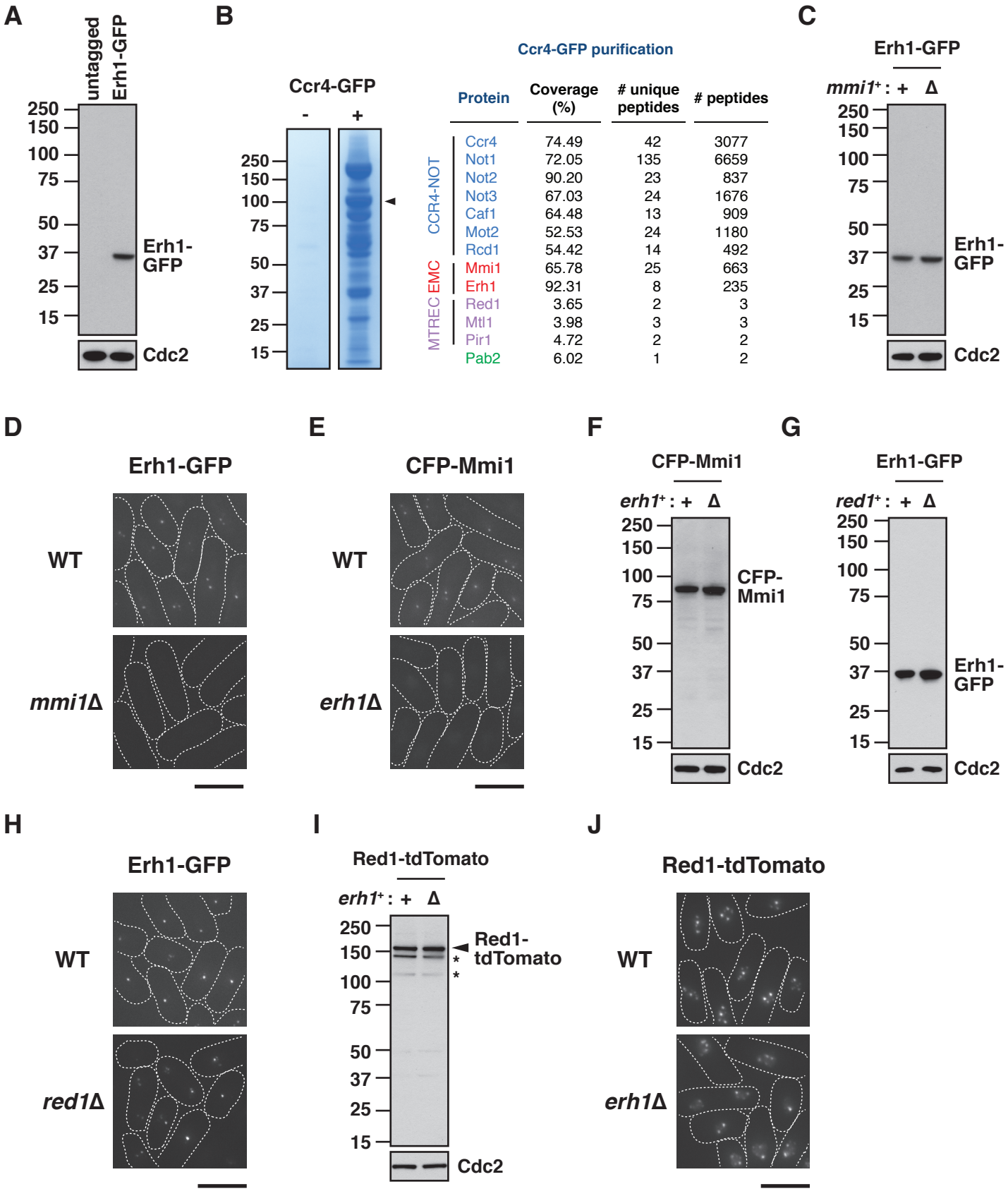
A
untagged
Erh1-GFP
250
150
100
75
50
37
25
15
Erh1-GFP
Cdc2
B
Ccr4-GFP
-
+
250
150
100
75
50
37
25
15
Ccr4-GFP purification
Protein
Coverage (%)
unique peptides
peptides
CCR4-NOT
Ccr4 74.49 42 3077
Not1 72.05 135 6659
Not2 90.20 23 837
Not3 67.03 24 1676
Caf1 64.48 13 909
Mot2 52.53 24 1180
Rcd1 54.42 14 492
MTREC EMC
Mmi1 65.78 25 663
Erh1 92.31 8 235
Red1 3.65 2 3
Mtl1 3.98 3 3
Pir1 4.72 2 2
Pab2 6.02 1 2
C
Erh1-GFP
mmi1+ : + Δ
250
150
100
75
50
37
25
15
Erh1-GFP
Cdc2
D
Erh1-GFP
WT
mmi1Δ
E
CFP-Mmi1
WT
erh1Δ
F
CFP-Mmi1
erh1+ : + Δ
250
150
100
75
50
37
25
15
CFP-Mmi1
Cdc2
G
Erh1-GFP
red1+ : + Δ
250
150
100
75
50
37
25
15
Erh1-GFP
Cdc2
H
Erh1-GFP
WT
red1Δ
I
Red1-tdTomato
erh1+ : + Δ
250
150
100
75
50
37
25
15
Red1-tdTomato
*
*
Cdc2
J
Red1-tdTomato
WT
erh1Δ

Figure S4. Ccr4 purification, expression and localization of Erh1, Mmi1 and Red1, related to Figure 4
(A) Western blots of Erh1-GFP. Protein extracts from parental untagged or Erh1-GFP strains were examined on Western blots probed with anti-GFP antibody. Cdc2 was also monitored as a loading control. (B) Ccr4-GFP purification. Extracts from the parental (untagged) or Ccr4-GFP strains were purified on anti-GFP agarose beads. Ccr4-binding proteins were visualized on an SDS-PAGE gel by CBB staining (left). The total peptide coverage (%), total number of unique peptides, and total number of peptides of the identified proteins are shown (right). (C) Western blots of Erh1-GFP. Protein extracts from wild-type (WT) or *mmi1*Δ strains expressing Erh1-GFP (C) were examined on Western blots probed with anti-GFP antibody. Cdc2 was also monitored as a loading control. (D and E) The localization of Erh1-GFP or CFP-Mmi1 in the indicated strains was determined by fluorescence microscopy. Representative images of WT and *mmi1*Δ strains expressing Erh1-GFP (D), and WT and *erh1*Δ strains expressing CFP-Mmi1 (E) are shown. The white dashed lines indicate the cell shape. Bars, 5 *μ*m. (F and G) Western blots of CFP-Mmi1 or Erh1-GFP in the indicated strains. Protein extracts from WT and *erh1*Δ strains expressing CFP-Mmi1 (F), and WT and *mmi1*Δ strains expressing Erh1-GFP (G) were examined on Western blots probed with anti-GFP antibody. Cdc2 was also monitored as a loading control. (H) The localization of Erh1-GFP in WT and *red1*Δ strains was examined by fluorescence microscopy. Representative images are shown, and the white dashed lines indicate the cell shape. Bars, 5 *μ*m. (I) Western blot analysis of Red1-tdTomato in WT and *erh1*Δ strains. Protein extracts from WT and *erh1*Δ strains expressing Red1-tdTomato were probed with anti-RFP antibody. Cdc2 was also monitored as a loading control. Bands marked with * presumably correspond to degradation products of Red1-tdTomato. (J) The localization of Red1-tdTomato in WT and *erh1*Δ strains was examined by fluorescence microscopy. Representative images are shown, and the white dashed lines indicate the cell shape. Bars, 5 *μ*m

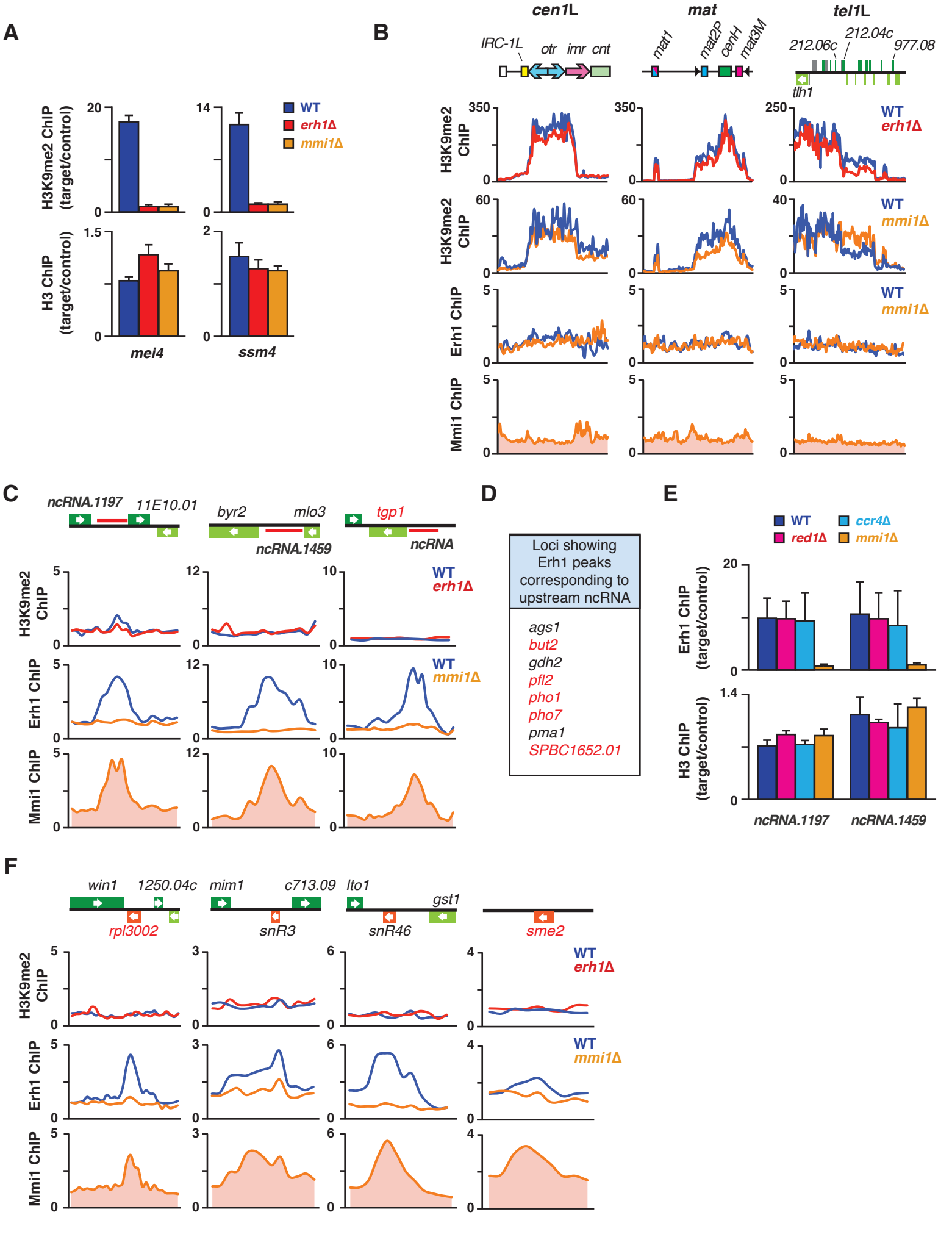
A
H3K9me2 ChIP (target/control)
H3 ChIP (target/control)
WT
erh1Δ
mmi1Δ
mei4
ssm4
B
cen1L
mat
tel1L
IRC-1L
otr
imr
cnt
mat1
mat2P
cenH
mat3M
212.06c
212.04c
977.08
tlh1
H3K9me2 ChIP
Erh1 ChIP
Mmi1 ChIP
C
ncRNA.1197
11E10.01
byr2
mlo3
ncRNA.1459
tgp1
ncRNA
D
Loci showing Erh1 peaks corresponding to upstream ncRNA
ags1
but2
gdh2
pfl2
pho1
pho7
pma1
SPBC1652.01
E
ccr4Δ
red1Δ
Erh1 ChIP (target/control)
H3 ChIP (target/control)
ncRNA.1197
ncRNA.1459
F
win1
1250.04c
mim1
c713.09
lto1
gst1
rpl3002
snR3
snR46
sme2

Figure S5. EMC is required for the assembly of heterochromatin islands, but not for constitutive heterochromatin formation, and localize to euchromatic domains, related to Figure 5

(A) EMC promotes heterochromatin assembly at the *mei4* and *ssm4* loci. Input and H3K9me2 ChIP DNA from the indicated strains were measured by real-time PCR (qPCR) using gene-specific primers, and H3K9me2 ChIP enrichment at *mei4* and *ssm4* was calculated relative to the enrichment at the control locus, *vps33*. Error bars indicate the SD from two independent experiments. (B) ChIP-chip results of H3K9me2 (WT and *erh1*Δ, WT and *mmi1*Δ), Erh1-GFP (WT and *mmi1*Δ) and CFP-Mmi1 at centromere 1L (*cen*1L), the mating-type locus (*mat*) and telomere 1L (*tel*1L). (C) ChIP-chip results of H3K9me2 (WT and *erh1*Δ), Erh1-GFP (WT and *mmi1*Δ) and CFP-Mmi1 at a non-coding RNA (ncRNA) upstream of *byr2*$^{+}$, *tgp1*$^{+}$ or *SPCC11E10.01*. Red bars indicate the positions of the ncRNAs. (D) Additional examples of genes that contain upstream ncRNAs with Erh1 enrichment. Genes in red are upregulated in *erh1*Δ cells. (E) Fold enrichment of Erh1-GFP (top) and H3 (bottom) at two ncRNA loci, which are devoid of significant H3K9me2, relative to the control locus, *vps33*. Data from three (Erh1 ChIP) or two (H3 ChIP) biological replicates are shown as the mean+SD. (F) ChIP-chip results of H3K9me2 (WT and *erh1*Δ), Erh1-GFP (WT and *mmi1*Δ) and CFP-Mmi1 at the indicated euchromatic loci such as *rpl3002*$^{+}$, snoRNAs and *sme2*$^{+}$ loci. Genes in red are upregulated in *erh1*Δ cells.

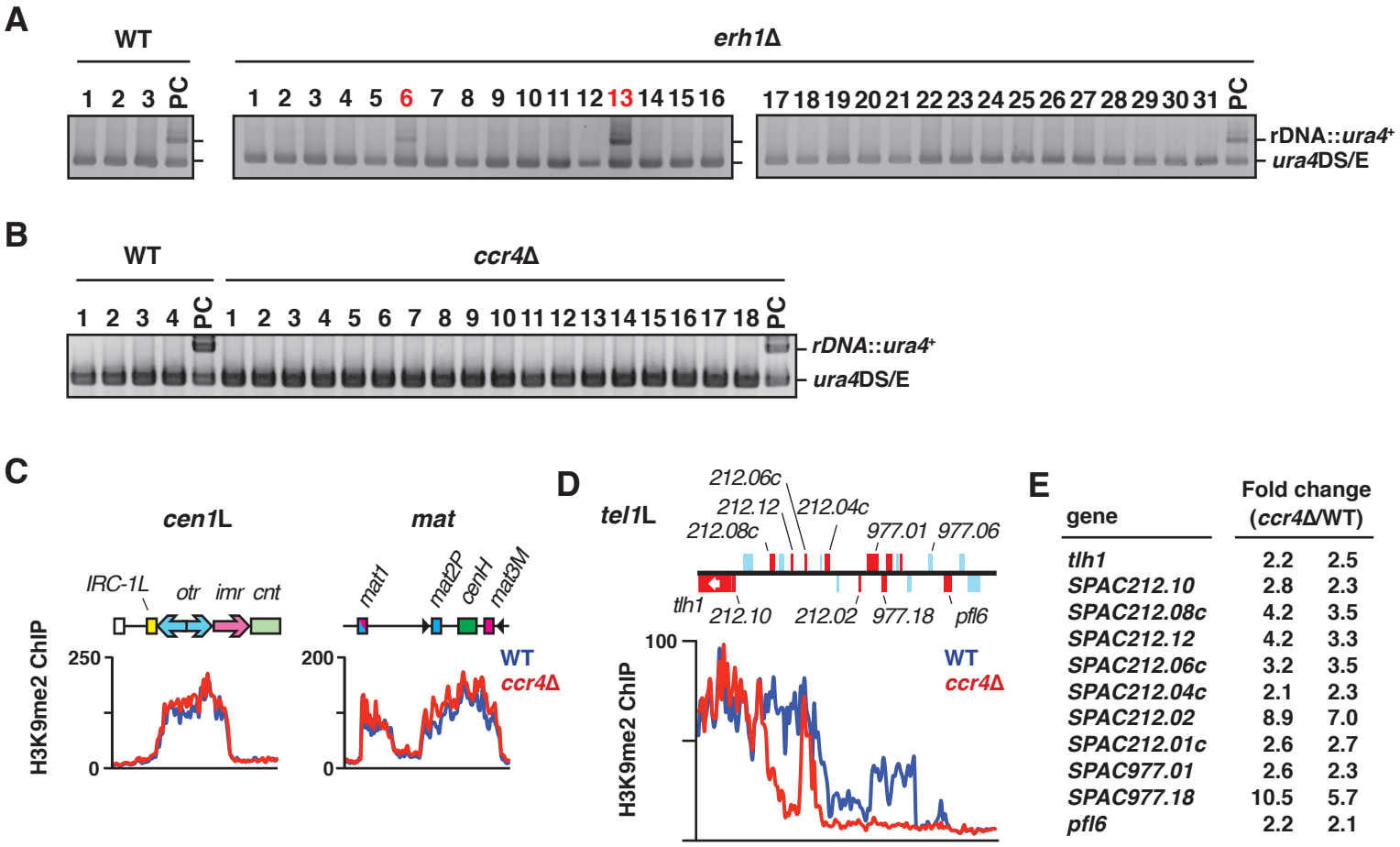

E

gene	Fold change (*ccr4*Δ/WT)	
tlh1	2.2	2.5
SPAC212.10	2.8	2.3
SPAC212.08c	4.2	3.5
SPAC212.12	4.2	3.3
SPAC212.06c	3.2	3.5
SPAC212.04c	2.1	2.3
SPAC212.02	8.9	7.0
SPAC212.01c	2.6	2.7
SPAC977.01	2.6	2.3
SPAC977.18	10.5	5.7
pfl6	2.2	2.1

Figure S6. Ccr4 is required for *rDNA* integrity and subtelomereic heterochromatin assembly, related to Figure 6

(A and B) Verification of *rDNA*::*ura4*$^+$ loss in WT, *erh1*Δ and *ccr4*Δ. The loss of *ura4*$^+$ in clones that do not grow on uracil-lacking plates was confirmed by genomic PCR. *ura4*DS/E, a *ura4*$^+$ minigene, served as an internal control for PCR. PC: positive control (starting strains used for this assay) for genomic PCR. Clone #6 and #13 of *erh1*Δ, indicated in red, have *ura4*$^+$, indicating these strains carry *ura4*$^+$ with a mutation, and do not lose the *ura4*$^+$ marker. Therefore, we considered these clones to be false positive. (C and D) Heterochromatin assembly is unaffected at centromeres and the *mat* locus, but is compromised at subtelomeres in *ccr4*Δ. ChIP-chip results of H3K9me2 at centromere 1L (*cen*1L) and the *mat* locus (*mat*) (C) and telomere 1L (*tel*1L) (D) in WT and *ccr4*Δ are shown. (E) List of genes at telomere 1L that are upregulated in *ccr4*Δ. The fold increase (*ccr4*Δ/WT) determined from two independent RNA-Seq data sets are shown.

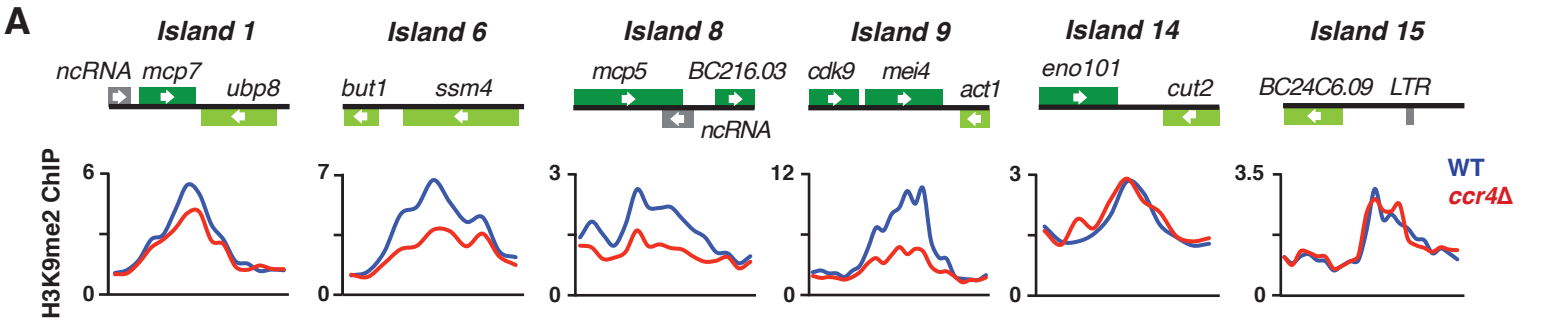

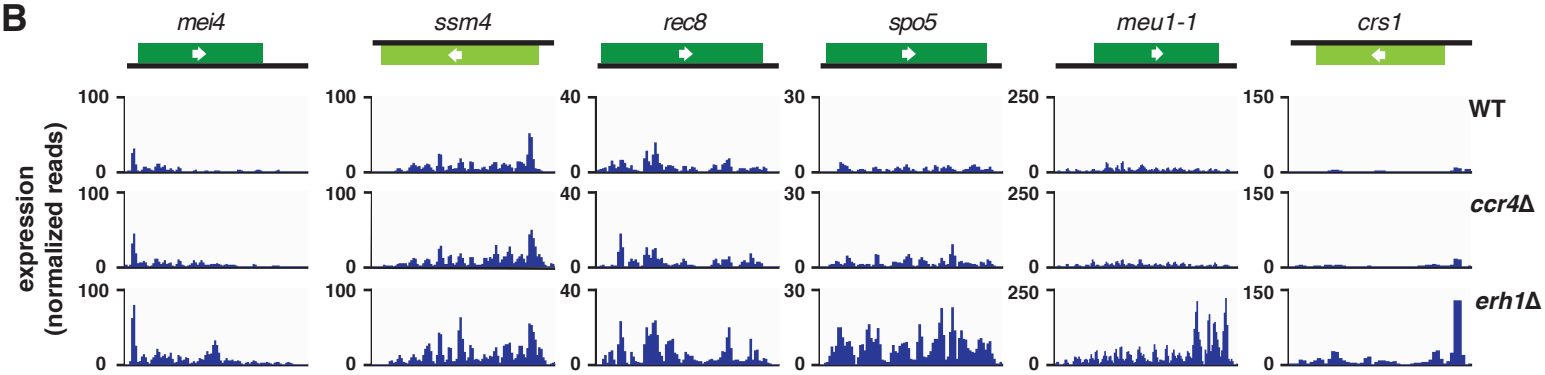

C

Fold change relative to WT

gene	*ccr4*Δ		*erh1*Δ	
mei4	1.0	0.8	5.3	5.2
rec8	0.9	0.9	3.1	3.3
ssm4	0.7	0.6	2.6	2.4
spo5	0.9	0.9	10.6	10.7
mcp5	1.2	1.0	6.2	6.7
rec10	0.9	1.0	9.2	9.5
crs1	0.8	0.8	15.7	14.4
sme2	2.2	2.9	3.5	4.3
ubi4	2.2	1.7	1.8	1.8

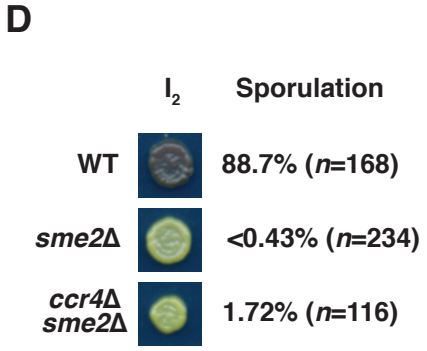

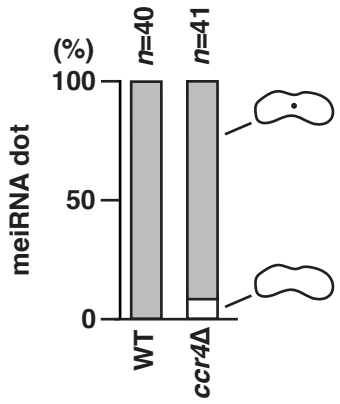

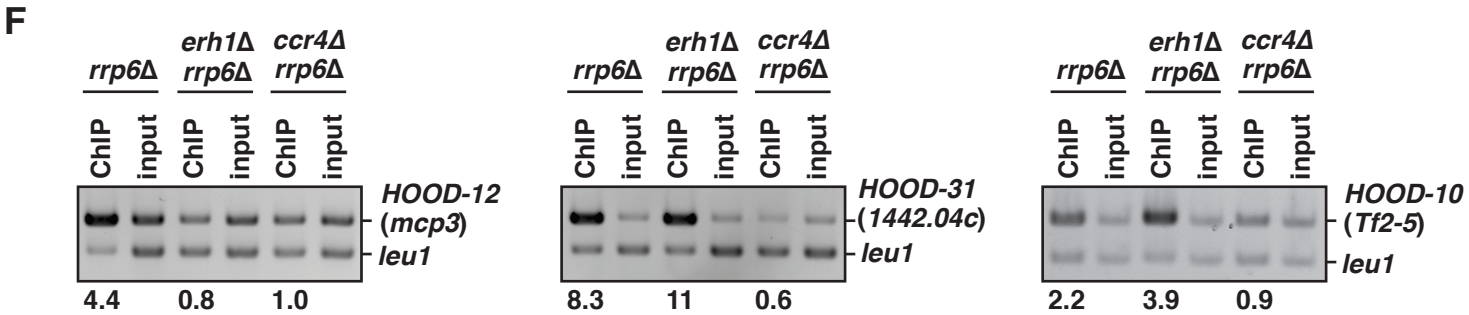

Figure S7. Ccr4 has an important role in HOOD assembly, but not in heterochromatin island assembly, meiotic mRNA degradation or meiRNA dot formation, related to Figure 7

(A) ChIP-chip results of H3K9me2 in WT and *ccr4*Δ at heterochromatin islands. (B) Expression levels of Erh1-target genes in WT, *ccr4*Δ and *erh1*Δ. RNA-Seq data of 6 representative meiotic mRNAs in WT, *ccr4*Δ and *erh1*Δ are shown. (C) Fold change of representative Mmi1-regulon genes in *ccr4*Δ and *erh1*Δ. (D) *ccr4*Δ does not significantly suppress the sporulation defect of *sme2*Δ. The homothallic *sme2*Δ strain was crossed with the homothallic *ccr4*Δ strain, followed by tetrad dissection. Dissected spores were grown on rich plates for 4 days, on minimal plates for 3 days, and then analyzed by iodine staining and microscopy. (E) Ccr4 is dispensable for meiRNA dot formation in meiotic cells. The meiRNA dot in meiotic *ccr4*$^{+}$ (WT) and *ccr4*Δ cells was visualized by the MS2 system and analyzed using a fluorescence microscope. The percentages of cells with 0 (white) or 1 (grey) meiRNA dot are shown in the bar graph. "*n*" indicates the number of cells examined for each strain. (F) Both EMC-dependent (*HOOD-12*) and EMC-independent HOOD (*HOOD-31* and *-10*) assembly is abolished in *ccr4*Δ. The H3K9me2 level at three loci relative to the level at the control *leu1* locus was determined by ChIP-multiplex PCR. Relative enrichment values (target/*leu1*) are also shown.

List of Supplemental Tables

SUPPLEMENTAL EXPERIMENTAL PROCEDURES

Strains and media

The general genetic methods used in this study were described previously (Moreno et al., 1991). Rich medium supplemented with adenine (YEA), rich but adenine-limited medium (YE), minimal medium (PMG), minimal medium without adenine (PMG-Ade), PMG without uracil (PMG-Ura) and AA lacking both leucine and uracil (AA-Leu-Ura) were used to grow yeast cells (Allshire et al., 1994; Moreno et al., 1991). Deletion strains and strains expressing tdTomato, mCherry (Shaner et al., 2004) and GFP (Ogawa et al., 2004) epitope-tagged proteins were constructed using PCR-based methods as described previously (Bahler et al., 1998).

RNA analyses

Total RNA was prepared using the MasterPure™ Yeast RNA purification kit (Epicentre). RNA-Sequencing library construction and analyses were described previously (Lee et al., 2013). The data from wild-type cells were compared with those from *erh1*Δ*, ccr4*Δ, *mmi1*Δ and *red1*Δ cells (Lee et al., 2013); a total of 7019 genes were examined, and the transcripts that showed more than a 2-fold increase or a 0.5-fold decrease were selected as "increased" or "decreased" transcripts, respectively. The increased or decreased genes in *erh1*Δ are listed in Tables S1 and S2, respectively. Note that we do not consider ribosomal rRNA results reliable in our RNA-Sequencing data for two reasons: (1) ribosomal RNA was actively removed during the library preparation step due to the overabundance of RNA originating from these loci; and (2) the high number of reads interfered with accurate quantitation and normalization of the loci. Collectively, this yielded inaccurate FPKM measurements. The statistical significance (*p*-value) of the overlap of two groups was determined by hypergeometric probability distribution.

Northern blotting for small RNAs was performed as described previously (Yamanaka et al., 2013). Briefly, small RNAs were purified from cells grown at 30°C (or 33°C for *pir2-1 rrp6*Δ and *rrp6*Δ in Figure 7F) using the *mir*Vana™ miRNA isolation kit (Life Technologies), resolved on a 15% TBE-urea acrylamide gel, and transferred to Hybond™-NX (GE Healthcare) followed by EDC chemical cross-linking. The blots were hybridized with ^{32}P-labelled single-strand RNA probes (~50 nucleotides) corresponding to *HOOD-12* (*mcp3*/*red1*/*och1*), *SPCC1442.04c* or *Tf2* in ULTRAhyb®-Oligo (Life Technologies) at 42°C.

Protein purification

Protein purification was performed as previously reported with some modifications (Sugiyama et al., 2007). Briefly, cells harvested from 4L cultures were flash frozen in liquid nitrogen and then crude cell lysates were prepared using a house-hold blender. The cell lysates were cleared by ultracentrifugation, and the cleared lysates were subjected to affinity-purification on anti-GFP agarose beads (antibodies-online). Beads were washed extensively, and purified proteins were eluted three times with 0.2 M glycine (pH 2.0). Then eluted proteins were precipitated with TCA (trichloroacetic acid) and resolved on 4-12% Bis-Tris Gel (Life Technologies). Proteins were visualized using SimplyBlue™ SafeStain (Life Technologies). To remove DNA/RNA molecules, Erh1-GFP bound on anti-GFP agarose beads were treated with 50 U/ml Benzonase® (Sigma-Aldrich) for 30 min after an extensive wash step. The anti-GFP agarose beads incubated with Benzonase® were subjected to a second extensive wash followed by protein elution with 0.2 M glycine (pH 2.0).

Mass spectrometry analysis

Mass spectrometry was performed as described previously (Lee et al., 2013). The protein search was performed against the UnitPro *Schizosaccharomyces pombe* database from the European Bioinformatics Institute. To compare the relative protein amounts in the Benzonase (-) and (+) samples, we used intensity-based absolute quantification (iBAQ) values (Schwanhausser et al., 2011) calculated by MaxQuant software (ver. 1.5.2.8). The iBAQ values of Erh1-associated proteins were normalized to the iBAQ value of the bait protein (Erh1-GFP) and indicated as a percentage of the bait. Unique and total peptide counts, iBAQ values and sequence coverage of identified proteins are shown in Tables S3-S5.

Co-immunoprecipitation and Western blotting

Co-immunoprecipitation was performed as described previously (Lee et al., 2013). The sample preparation for Western blotting was performed using an alkaline protein extraction method (Matsuo et al., 2006) or a TCA extraction method (Sugiyama and Sugioka-Sugiyama, 2011). Anti-GFP (7.1 and 13.1, Roche), anti-RFP (PM005, MBL), and anti-Cdc2 (Y100.4, Santa Cruz) antibodies were used for probing Erh1-GFP, CFP-Mmi1, Red1-tdTomato and Cdc2.

ChIP and ChIP-chip

ChIP and ChIP-chip experiments were carried out as previously described (Lee et al., 2013). Strains were grown at 30°C (or 33°C for *pir2-1 rrp6*Δ and *rrp6*Δ in Figure 7E). Anti-H3K9me2 (ab1220, Abcam; ab115159, Abcam), anti-GFP (ab290, Abcam) and anti-H3 (ab1791, Abcam) antibodies and proteinA/G magnetic beads (Life Technologies or NEB) were used to precipitate protein-chromatin complexes. Immunoprecipitated DNA and input DNA were analyzed by multiplex PCR using AmpliTaq® DNA Polymerase (Thermo Fisher Scientific), real-time PCR using SYBR® *Premix Ex Taq*™ II (TaKaRa Bio) and DNA Engine Opticon®2 System (BioRad), or labeled with Cy5/Cy3 and used for microarray-based ChIP-chip analysis by hybridization to a custom 4×44K oligonucleotide array according to Agilent's recommended procedure. ChIP-qPCR experiments were repeated at least twice, and ChIP-chip experiments were repeated twice.

Supplemental References

Allshire, R.C., Javerzat, J.P., Redhead, N.J., and Cranston, G. (1994). Position effect variegation at fission yeast centromeres. Cell 76, 157-169.

Bahler, J., Wu, J.Q., Longtine, M.S., Shah, N.G., McKenzie, A., 3rd, Steever, A.B., Wach, A., Philippsen, P., and Pringle, J.R. (1998). Heterologous modules for efficient and versatile PCR-based gene targeting in *Schizosaccharomyces pombe*. Yeast 14, 943-951.

Lee, N.N., Chalamcharla, V.R., Reyes-Turcu, F., Mehta, S., Zofall, M., Balachandran, V., Dhakshnamoorthy, J., Taneja, N., Yamanaka, S., Zhou, M., et al. (2013). Mtr4-like protein coordinates nuclear RNA processing for heterochromatin assembly and for telomere maintenance. Cell 155, 1061-1074.

Matsuo, Y., Asakawa, K., Toda, T., and Katayama, S. (2006). A rapid method for protein extraction from fission yeast. Biosci. Biotechnol. Biochem. 70, 1992-1994.

Moreno, S., Klar, A., and Nurse, P. (1991). Molecular genetic analysis of fission yeast *Schizosaccharomyces pombe*. Methods Enzymol. 194, 795-823.

Ogawa, H., Yu, R.T., Haraguchi, T., Hiraoka, Y., Nakatani, Y., Morohashi, K., and Umesono, K. (2004). Nuclear structure-associated TIF2 recruits glucocorticoid receptor and its target DNA. Biochem. Biophys. Res. Commun. 320, 218-225.

Schwanhausser, B., Busse, D., Li, N., Dittmar, G., Schuchhardt, J., Wolf, J., Chen, W., and Selbach, M. (2011). Global quantification of mammalian gene expression control. Nature 473, 337-342.

Shaner, N.C., Campbell, R.E., Steinbach, P.A., Giepmans, B.N., Palmer, A.E., and Tsien, R.Y. (2004). Improved monomeric red, orange and yellow fluorescent proteins derived from *Discosoma* sp. red fluorescent protein. Nat. Biotechnol. 22, 1567-1572.

Shobuike, T., Tatebayashi, K., Tani, T., Sugano, S., and Ikeda, H. (2001). The *dhp1*$^{+}$ gene, encoding a putative nuclear 5'→3' exoribonuclease, is required for proper chromosome segregation in fission yeast. Nucleic Acids Res. 29, 1326-1333.

Sugiyama, T., Cam, H.P., Sugiyama, R., Noma, K., Zofall, M., Kobayashi, R., and Grewal, S.I. (2007). SHREC, an effector complex for heterochromatic transcriptional silencing. Cell 128, 491-504.

Sugiyama, T., and Sugioka-Sugiyama, R. (2011). Red1 promotes the elimination of meiosis-specific mRNAs in vegetatively growing fission yeast. EMBO J. 30, 1027-1039.

Thon, G., and Verhein-Hansen, J. (2000). Four chromo-domain proteins of *Schizosaccharomyces pombe* differentially repress transcription at various chromosomal locations. Genetics 155, 551-568.

Yamanaka, S., Mehta, S., Reyes-Turcu, F.E., Zhuang, F., Fuchs, R.T., Rong, Y., Robb, G.B., and Grewal, S.I. (2013). RNAi triggered by specialized machinery silences developmental genes and retrotransposons. Nature 493, 557-560.